SEMARAK ILMU PUBLISHING

Journal of Advanced Research in Fluid Mechanics and Thermal Sciences

Journal homepage:
https://semarakilmu.com.my/journals/index.php/fluid_mechanics_thermal_sciences/index
ISSN: 2289-7879

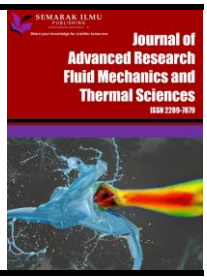

Effects of Hall Current, Activation Energy and Diffusion Thermo of MHD Darcy-Forchheimer Casson Nanofluid Flow in the Presence of Brownian Motion and Thermophoresis

Ramachandra Reddy Vaddemani[1,*], Sreedhar Ganta[1], Raghunath Kodi[2]

[1] Department of Humanities and Sciences, K.S.R.M College of Engineering, Kadapa-516003, Andhra Pradesh, India
[2] Department of Humanities and Sciences, St. Johns College of Engineering Technology, Yemmiganur-518360, Andhra Pradesh, India

ARTICLE INFO

Article history:
Received 3 January 2022
Received in revised form 10 April 2023
Accepted 16 April 2023
Available online 4 May 2023

Keywords:
Hall current; diffusion thermos; activation energy; MHD; heat generation; Casson fluid

ABSTRACT

The present article is about the study of Darcy-Forchheimer flow of Casson nanofluid over a linear stretching surface. Effects like variable Hall current, activation energy, Diffusion thermo is also incorporated for the analysis of heat and mass transfer. The governing nonlinear partial differential equations (PDEs) with convective boundary conditions are first converted into the nonlinear ordinary differential equations (ODEs) with the help of similarity transformation, and then the resulting nonlinear ODEs are solved with the help of shooting method. The impact of different physical parameters like Activation energy, Diffusion thermo, Brownian motion, thermophoresis parameter, hall current, magnetic parameter, nonlinear radiative heat flux, Prandtl number, Lewis number, reaction rate constant, on Nusselt number, velocity, temperature and concentration profile has been discussed. It is viewed that the fluid velocity and concentration profile enhance with increasing hall parameter and Activation energy respectively.

1. Introduction

Type of material having pores is called porous media, where the pores are usually filled with fluid. The concept of fluid flow in porous media is of great interest for engineers, mathematicians, geologists and architectures due to its diverse applications, like the flow of water in reservoirs, heat exchanger, oil production and catalytic reactors etc. The process of heat transfer in porous media has abundantly been used in the production of papers, non-woven materials, heat pipe technology, electronic technology and energy storage etc. [1-4]. In 1856, Henry Darcy, a French civil engineer, laid the foundation of flow of homogeneous fluids through porous media during his work on flow of water through sand beds. Darcy law cannot work well when inertial and boundary effects take place at higher flow rate. Later on, in 1901, Forchheimer [5], a Dutch scientist, extended the Darcian velocity expression by adding the square velocity term in the momentum equation for the prediction of the behavior of inertia and boundary layer flow. The name 'Forchheimer term' was later coined by

* *Corresponding author.*
E-mail address: vrcreddymaths77@gmail.com

https://doi.org/10.37934/arfmts.105.2.129145

Muskat [6] considered the Darcy-Forchheimer model over stretching surface and concluded that an increase in the value of electric field parameter results in decreasing the nanoparticle concentration profile.

The use of magnetic field of high intensity to an ionic liquid having less density, the conduction normal to the magnetic field is converted to curling of atomic particles and ions related to magnetic lines of force before occurring the clashing and a current induced perpendicular to both the electric and magnetic fields, is known as Hall effect. This effect is considered with heat or mass transfer analysis under the situation where the effect of the electromagnetic force is strong. Hall current is most prominent on the absolute value and orientation of the current density and thereby on the magnetic force term. Under the effects of Hall currents the convective flow problem with magnetic field is significant in view of engineering uses in electric transformers, transmission lines, refrigeration coils, power generators, MHD accelerators, nanotechnological processing, nuclear energy systems exploiting fluid metals, blood flow control and heating elements. In case of magnetic field of high strength and less density of the gas, the investigation of magnetohydrodynamic flows with Hall current have the best utilizations in the study of Hall accelerators and flight magnetohydrodynamic. Peristaltic flows have vast applications under the effects of applied magnetic field in the magnetohydrodynamic feature of blood, process of dialysis, oxygenation and hypothermia. Exploration of non-Newtonian fluid flows has been the focus of many scientists due to its vast applications in industries and engineering. Important applications are existed in food engineering, petroleum production, power engineering, in polymer solutions and in melt in the plastic processing industries. Hall effect plays an important role when the Hall parameter is high. Hall parameter is the ratio of electron cyclotron frequency to atom-electron collision frequency. So, the Hall current effect is high when the electron-atom collision frequency is low. The chemically reactive second grade via porous saturated space was investigated by Kodi *et al.,* [7] using a perturbation technique. Raghunath *et al.,* [8] have investigated the effects of Soret, Rotation, Hall, and Ion Slip on the unsteady flow of a Jeffrey fluid through a porous medium. Raghunath and Mohanaramana [9] have researched Hall, Soret, and rotational effects on unsteady MHD rotating flow of a second-grade fluid through a porous media in the presence of chemical reaction and aligned magnetic field. Ramudu *et al.,* [10] studied Heat and Mass transfer in MHD Casson nanofluid flow past a stretched sheet with thermophoresis and Brownian motion.

Thermo-diffusion is a transport process in which the particles are transported to a mixture of several factors determined through the temperature gradient. As heat and mass transfer occurs in fluid motion, the driving potential and flow resistance become more complex. This results in a continuous difference within the concentration of one species in the chemical process relative to the other species. Thanks to its wide range of applications in heat exchangers for packed beds, heat insulation, energy storage devices, drying technology, nuclear waste repositories, catalytic reactors, and geothermal systems, the mass and heat transport in porous media is further enhanced by investigations experimentally and theoretically. Cheng [11] examined the impacts of Dufour and Soret of a heated plate on viscous liquid flow. Hayat *et al.,* [12] considered the impacts of Dufour and Soret on the stretching sheet of the hyperbolic tangent fluid. Hayat *et al.,* [12] examined the variation in diffusionthermal and thermal-diffusion within the convective flow to the stretching layer of a second-grade liquid. The thermal and mass transfer characteristics of the naturally produced convection on the vertical surface of the saturated porous substance linked to a magnetic field, considering Dufour and Soret effects, have been numerically investigated by Postelnicu [13]. Kafoussias and Williams [14] considered boundary layer streams for mixed forced-natural convection in the existence of Soret and Dufour related to thermodiffusion and diffusion-thermo effects. Considering the Dufor and Soret effects by Alam *et al.,* [15] theoretically, a steady 2D heat free and

mass transfer flow passes through a continuous semi-infinite vertical porous plate on a porous medium. Weaver and Viskanta [16] figured out that the coupling interaction is important when the difference in temperature and concentration is high or the difference in the molecular mass of the two elements is high in the binary mix.

Magnetic nanofluids is another imperative sub branch of nanofluids as it has momentous contribution in number of industrial and engineering fields. Hydrodynamic characteristics and heat transfer rate is further manipulated when the magnetic field is applied across the flow of nanofluids. Often aluminum oxide and magnetite are oppressed during the formulation of such fluids. Sheikholeslami *et al.,* [17] investigated the force convection heat transfer of magnetic nanofluids flow in a lid driven semi-annulus enclosure. They used the two phase model for the simulation of nanofluids. They concluded that higher values of Lewis and Hartmann number decrease the rate of heat flux, but it is augmented for the larger values of Reynolds number. Abbasi *et al.,* [18] considered the boundary layer flow of two dimensional Jeffrey nanofluid with hydromagnetic effects over a linearly stretched sheet.

The process of irregular heat generation or absorption has widespread significances in biomedical and many engineering activities such as radial diffusers, the intention of thrust bearing, and crude oil recovery. Polymer processing, space technology, production of glass and heating a room by the open hearth fireplace are some useful industrial and engineering application of radiation. Abel and Nandeppanavar [19] have investigated the impact of variable heat absorption/generation on magnetohydrodynamic flow of non-Newtonian liquid across a stretching surface. It was reported that the local Nusselt number is reduced when the irregular heat source/sink parameters are increased. Sandeep and Sulochana [20], Sandeep [21], Kumar *et al.,* [22], and Ramadevi *et al.,* [23] examined the combined influence of thermal and mass transfer features of non-Newtonian liquids due to stretching of a surface. A numerical treatment was presented with the aid of fourth order Runge-Kutta method (RKF-4). It is also noted that the heat sink/source parameters control the mass and thermal performances. Mahanthesh *et al.,* [24] investigated the heat and mass transfer attributes on MHD viscoelastic fluid flow across a stretching surface with thermophoresis and Brownian motion. The impacts of nonlinear radiation, Brownian motion, and quartic chemical reaction on MHD bioconvective flow of nanofluid over an upper horizontal surface of paraboloid revolution were investigated by Makinde and Animasaun [25], who was reported that the Brownian motion increases concentration bulk fluid while thermophoresis declines it.

Thermophoresis is a process in which the fluid particles move towards a cooler region from the warmer [26]. This movement occurs because molecules from the warmer region having high kinetic energy impinge with the molecules having low energy in the cooler region. The velocity gained by the particles is thermophoresis velocity and the force experienced by the particles is called the thermophoresis force [27]. Particles deposition due to thermophoresis was measured accurately by Tsai *et al.,* [28]. Applications of thermophoresis can be seen in aerosol technology, radioactive particle expulsion in the nuclear reactor safety simulation, heat exchanger corrosion and deposition of silicon thin film. Layers of glass (SiO_2 and GeO_2) are built up by the deposition of particles on the tube wall with the help of modified chemical vapour deposition process. For very small sized chips, the potential failures increase due to the micro contamination by the particle deposition. The process of thermophoresis can be used to inhibit the deposition of small particles on the electronic chips for the purpose of efficiency. The thermophoresis transport of particles in one-dimensional flow for the thermophoresis velocity was studied first time by Goldsmith and May [29]. A theoretical analysis of thermophoresis of aerosol particles in the laminar flow over a horizontal flat plate was presented by Goren [30].

Motivated by the above studies and applications, the present work examines the effect of Hall Current, Activation energy and Diffusion thermo on MHD heat and mass transfer Casson Nanofluid flow with inclined plates in the presence of Brownian motion and Thermophoresis. The effects of flow regulating parameters on the distributions of flow are presented in tabular and graphical form. This consideration has an important value in engineering and biological research. Analytical and numerical approaches are applied to examine the modeled problem and also compared each other, and good results were obtained.

2. Non-Newtonian Casson Fluid Model

The following rheological equation is used to construct the governing equations for squeezing flow of Casson fluid between two parallel plates

$$\tau_{ij} = \begin{cases} 2\left(\mu_B + \dfrac{P_y}{\sqrt{2\pi}}\right) e_{ij}, \pi > \pi_{c,} \\ 2\left(\mu_B + \dfrac{P_y}{\sqrt{2\pi_C}}\right) e_{ij}, \pi < \pi_{c,} \end{cases} \tag{1}$$

In Eq. (1), $\pi = e_{ij}, e_{ij}$, where e_{ij} are the $(i, j)\,th$ Component of the deformation rate, π is the product of the deformation rate with itself, π_C is a critical value of this product based on the non-Newtonian model, μ_B is the plastic dynamic viscosity of the non-Newtonian fluid and P_y the yield stress of the fluid.

$$P_y = \frac{\mu_B \sqrt{2\pi}}{\beta} \tag{2}$$

Denote the yield stress of fluid. Some fluids require a gradually increasing shear stress to maintain a constant strain rate and are called Rheopectic, in the case of Casson fluid (Non-Newtonian) flow where $\pi > \pi_c$

$$\mu = \mu_B + \frac{p_y}{\sqrt{2\pi}} \tag{3}$$

Substituting Eq. (2) into Eq. (3), then, the kinematic viscosity can be written as

$$\vartheta = \frac{\mu}{\rho} = \frac{\mu_B}{\rho}\left(1 + \frac{1}{\beta}\right) \tag{4}$$

where $\beta = \dfrac{\mu_B \sqrt{2\pi_c}}{p_y}$ denotes the Casson fluid parameter. The nature of Non-Newtonian fluid vanishes and it behaves as Newtonian fluid when $\beta \to \infty$.

3. Formulation of the Problem

Consider steady heat and mass transfer of an incompressible hydromagnetic nanofluid flow along a vertical stretching sheet coinciding with the plane y = 0, has been considered in the presence of the Hall current effects. By keeping the origin fixed, two opposite and equal forces are assumed to employ along the x-axis so that the sheet stretches linearly in both positive and negative direction (see Figure 1).

i. With the assumption that the Newtonian nanofluid be electrically conducting and heat generating/absorbing, a strong magnetic field has been imposed normal to the direction of flow.
ii. Moreover, no electric field has been assumed to apply and the frequency of atom-electron collision has also been considered high for the generation of Hall current effect [31].
iii. Due to the strong magnetic flux density B_0, the Hall current effect is taken into consideration, however the small magnetic Reynolds number is employed and the induced magnetic field is ignored.
iv. Hall current effect is strong enough to give rise to a force in the z−direction and a cross flow is induced in the same direction which causes a three dimensional flow.
v. It is further assumed that there are no variations in the flow, heat and mass transfer in the z-direction.
vi. This assumption can be achieved by taking the sheet of infinite width. Non-conducting plate is considered so that the generalized Ohm's law gives J_y=0 in the flow field [32].
vii. Brownian motion and thermophoresis effects are considered using the Buongiorno model for the nanofluid [33]. Further, the effects of viscous dissipation and Joule heating are ignored.

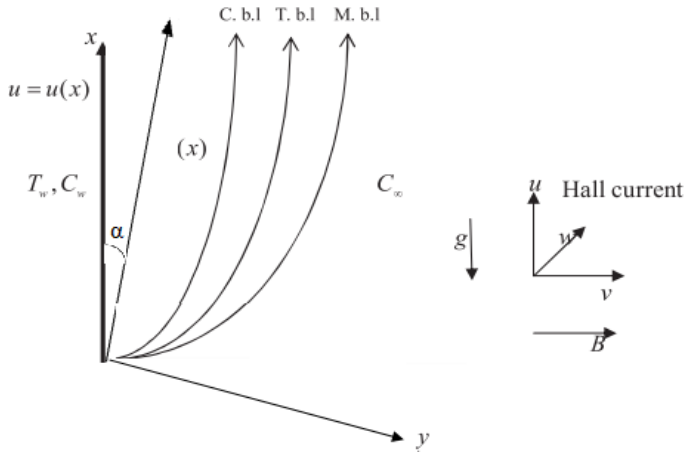

Fig. 1. Physical configuration

By the above mentioned assumptions and Boussinesq approximation, the mathematical form of the problem is

$$\frac{\partial u}{\partial x}+\frac{\partial u}{\partial y}=0 \tag{5}$$

$$u\frac{\partial u}{\partial x}+\upsilon\frac{\partial u}{\partial y}=\nu\left(1+\frac{1}{\beta}\right)\frac{\partial^2 u}{\partial y^2}-\frac{\sigma B_0^2}{\rho\left(1+m^2\right)}\left(mw+u\right)+g_C\beta_T(T-T_\infty)\ Cos\alpha+ g_C\beta_C(C-C_\infty)\ Cos\alpha-\frac{C_p}{x\sqrt{K^*}}u^2 \tag{6}$$

$$u\frac{\partial w}{\partial x}+\upsilon\frac{\partial w}{\partial y}=\nu\left(1+\frac{1}{\beta}\right)\frac{\partial^2 w}{\partial y^2}+\frac{\sigma B_0^2}{\rho\left(1+m^2\right)}\left(mu-w\right) \tag{7}$$

$$u\frac{\partial T}{\partial x}+\upsilon\frac{\partial T}{\partial y}=\frac{k}{\rho C_p}\frac{\partial^2 T}{\partial y^2}+\frac{q^m}{\rho C_p}+\tau\left(D_B\frac{\partial C}{\partial y}\frac{\partial T}{\partial y}+\frac{D_T}{T_\infty}\left(\frac{\partial T}{\partial y}\right)^2\right)-\frac{1}{\rho C_p}\frac{\partial q_r}{\partial y}+\frac{D_m k_T}{c_s c_p}\frac{\partial^2 C}{\partial y^2} \tag{8}$$

$$u\frac{\partial C}{\partial x}+\upsilon\frac{\partial C}{\partial y}=D_B\frac{\partial^2 C}{\partial y^2}-k_r^2\left(C-C_\infty\right)\left(\frac{T}{T_\infty}\right)^m\exp\left(\frac{-E_a}{K^*T}\right) \tag{9}$$

where q^m indicates the coefficient of internal heat absorption by Chamkha and Khaled [34] and Abo-Eldahab and El Aziz [35], it follows that

$$q^m=\left(\frac{ka}{\nu}\right)\left[A^*(T_w-T_\infty)e^{-\eta}+B^*(T-T_\infty)\right] \tag{10}$$

When both A^* and B^* are positive, we have the heat generation case whereas for the negative values of both of them, there is the internal heat absorption.

The corresponding boundary conditions for the governing PDEs are

$$\begin{aligned} &u=ax,\quad \upsilon=0,\quad w=0,\quad T=T_w,\quad C=C_w && \text{at } y=0\\ &u\to 0,\quad \upsilon\to 0,\quad w\to 0,\quad T\to T_\infty\quad C\to C_\infty && \text{as } y\to\infty \end{aligned} \tag{11}$$

The radiative heat flux q_r (using Roseland approximation followed Mahanthesh *et al.,* [24]) is defined as

$$q_r=-\frac{4\sigma^*}{3K^*}\left(\frac{\partial T^4}{\partial y}\right) \tag{12}$$

We assume that the temperature variances inside the flow are such that the term T^4 can be represented as linear function of temperature. This is accomplished by expanding T^4 in a Taylor series about a free stream temperature T_∞ as follows.

$$T^4=T_\infty^4+4T_\infty^3\left(T-T_\infty\right)+6T_\infty^2\left(T-T_\infty\right)^2+..... \tag{13}$$

After neglecting higher-order terms in the above equation beyond the first degree term in $\left(T-T_{\infty}\right)$, we get

$$T^4 \cong 4T_{\infty}^3 T - 3T_{\infty}^4 \tag{14}$$

Thus substituting Eq. (14) in Eq. (12), we get

$$q_r = -\frac{16T_{\infty}^3\sigma^*}{3K^*}\left(\frac{\partial T}{\partial y}\right) \tag{15}$$

Using Eq. (15), Eq. (7) can be written as

$$u\frac{\partial T}{\partial x}+\upsilon\frac{\partial T}{\partial y}=\frac{k}{\rho C_p}\frac{\partial^2 T}{\partial y^2}+\frac{q^m}{\rho C_p}+\tau\left(D_B\frac{\partial C}{\partial y}\frac{\partial T}{\partial y}+\frac{D_T}{T_{\infty}}\left(\frac{\partial T}{\partial y}\right)^2\right) + \frac{1}{\rho C_p}\frac{16T_{\infty}^3\sigma^*}{\partial K^*}\left(\frac{\partial^2 T}{\partial y^2}\right)+\frac{D_m k_T}{c_s c_p}\frac{\partial^2 C}{\partial y^2} \tag{16}$$

The similarity transformation used to transform the PDEs to dimensionless ODEs

$$\eta=\sqrt{\frac{a}{\nu}}y,\ \psi(x,y)=\sqrt{a\nu}\,x\,f(\eta),\ w=axg(\eta)\ \ \phi(\eta)=\frac{C-C_{\infty}}{C_w-C_{\infty}},\ \theta(\eta)=\frac{T-T_{\infty}}{T_w-T_{\infty}} \tag{17}$$

Substitute Eq. (17) into Eq. (6), Eq. (7), Eq. (8), Eq. (9) and Eq. (10) yields to obtain the subsequent non dimensional equations.

$$\left(1+\frac{1}{\beta}\right)f'''+ff''-f'^2+Gr_x\theta Cos\alpha+Gr_c\phi Cos\alpha-\frac{M}{1+m^2}\left(f'+mg\right)-F_r\left(f''\right)^2=0 \tag{18}$$

$$\left(1+\frac{1}{\beta}\right)g''+fg'-f'g+\frac{M}{1+m^2}\left(mf'-g\right)=0 \tag{19}$$

$$\theta''\left(1+R_d\right)+\Pr f\theta'+\Pr N_b\left(\theta'\phi'+\frac{N_t}{N_b}\theta'^2\right)+A^*e^{-\eta}+B^*\theta+\Pr D_u\phi'=0 \tag{20}$$

$$N_b\phi''+\Pr\ N_bL_e\,f\,\phi'-N_bK_E\left(1+\theta\right)^m\varphi\exp\left(\frac{-E}{1+\theta}\right)=0 \tag{21}$$

The correlated Dimensionless boundary conditions (BCs) are

$$\begin{aligned} &f(0)=0, \quad f'(0)=1, \quad g(0)=0, \quad \theta(0)=0, \quad \phi(0)=1 \qquad at \quad \eta=0 \\ &f'(\eta)\to 0, \quad g(\eta)\to 0, \quad \theta(\eta)\to 0, \quad \phi(\eta)\to 0 \qquad as \quad \eta\to\infty \end{aligned} \tag{22}$$

In the equations that do not include dimensions, the important parameters are defined as

$$\begin{aligned} &M=\frac{\sigma B_0^2}{\rho a}, \quad \Pr=\frac{\nu}{\alpha}=\frac{\nu\rho C_p}{k}, \quad L_e=\frac{\alpha}{D_B}, \quad Gr_x=\frac{g_c\beta_T(T_w-T_\infty)}{a^2x} \\ &N_b=\frac{\tau D_B}{\nu}(C_w-C_\infty), \quad N_t=\frac{\tau D_T}{T_\infty\nu}(T_w-T_\infty), \quad Gr_C=\frac{g_c\beta_C(C_w-C_\infty)}{a^2x} \\ &Du=\frac{D_M k_T(C_w-C_\infty)}{C_S C_p \nu a^2(T_w-T_\infty)}, SK_E=\frac{k_r^2}{c}, R_d=\frac{14\sigma^* T_\infty^3}{3kK^*}, F_r=\frac{C_p}{\sqrt{K}} \end{aligned} \tag{23}$$

4. Physical Quantities of Interests

The local skin friction coefficient in the direction of x Cf_x, and in the direction of z Cf_z, the local Nusselt number Nu_x, and the local Sherwood number Sh_x are the physical quantities of relevance that influence the flow. These numbers have the following definitions

$$C f_x=\frac{2\tau_{wx}}{\rho(ax)^2}, \quad Cf_z=\frac{2\tau_{wz}}{\rho(ax)^2}, \quad Nu_x=\frac{xq_w}{k(T_w-T_\infty)}, \quad Sh_x=\frac{x\,j_w}{D_B(C_w-C_\infty)} \tag{24}$$

where τwx, τwy, qw and jw are the wall skin friction, wall heat flux and wall mass flux respectively given by

$$\tau_{wx}=\mu\left[\frac{\partial u}{\partial y}\right]_{y=0}, \quad \tau_{wz}=\mu\left[\frac{\partial w}{\partial y}\right]_{y=0}, \quad q_w=-k\left[\frac{\partial T}{\partial y}\right]_{y=0}, \quad j_w=-D_B\left[\frac{\partial C}{\partial y}\right]_{y=0} \tag{25}$$

The coefficient of skin friction, the Nusselt number, and the Sherwood number are all expressed in their non-dimensional versions in terms of the similarity variable as follows

$$Cf_x\,\mathrm{Re}_x^{1/2}=2f''(0), \quad Cf_z\,\mathrm{Re}_x^{1/2}=2g'(0), \quad Nu_x\,\mathrm{Re}_x^{-1/2}=-\theta'(0), \quad Sh_x\,\mathrm{Re}_x^{-1/2}=-\phi'(0) \tag{26}$$

5. Solution Methodology

The non-linear ODE system (14–17), susceptible to constraints 18, was solved using the shooting technique for various values of the related parameters. We were able to figure out from the graphs that the behavior of the solutions does not change much when the value is greater than 8. Because of this, and based on the results of the computational experiments described above, we are considering using the range [0,8] as the domain of the issue rather than the range [0,∞].We denote f by y_1, g by y_4, θ by y_6 and ϕ by y_8 for converting the boundary value problem (14-18) to the following initial value problem consisting of 9 first order differential equations.

$y_1'=y_2$,

$$y_2' = y_3,$$

$$y_3' = \left(\frac{1}{\left(1+\frac{1}{\beta}\right)}\right)\left[-y_1 y_3 + y_2^2 - Gr_x y_6 - Gr_c y_8 + \frac{M}{1+m^2}\left(y_2 + m y_4\right) - F_r\left(y_2\right)''\right],$$

$$y_4' = y_5,$$

$$y_5' = \left(\frac{1}{\left(1+\frac{1}{\beta}\right)}\right)\left(y_2 y_4 - y_1 y_5 - \frac{M}{1+m^2}\left(-y_4 + m y_2\right)\right),$$

$$y_6' = y_7,$$

$$y_7' = \left(\frac{1}{1+R_d}\right)\left[-\Pr y_1 y_7 - \Pr N_b\left(y_9 y_7 + \frac{N_t}{N_b} y_7^{\,2}\right) - A^* e^{-\eta} - B^* y_6 - \Pr D_u y_9\right],$$

$$y_8' = y_9,$$

$$y_9' = -N_b \Pr L_e y_1 y_9 + N_b K_E\left(1+y_6\right)^m \exp\left(\frac{-E}{1+y_6}\right) y_8$$

6. Results and Discussions

To envision the effect of various physical parameters on tangential velocity $f^i(\eta)$, transverse velocity $g(\eta)$, nanoparticle concentration $\phi(\eta)$ and temperature $\theta(\eta)$ profiles, Figure 2 to Figure 26 are plotted. In all these computations, unless mentioned, otherwise we have considered Nb= 0.3, $\alpha=\pi/3$, Nt= 0.7, Pr= 0.71, Le = 0.6, M= 0.5, m= 0.2, Grx = 0.5, Gr = 0.5, A^*=0.01, B^*= 0.01, Rd=0.5, E=1.0, σ=0.5, Fr=0.5, Du=1.0

Figure 2 and Figure 3 illustrate the impacts of the Inclined parameter α on tangential velocity $f^i(\eta)$, transverse velocity $g(\eta)$, and temperature $\theta(\eta)$ profiles, respectively. It is observed that both the velocity $f'(\eta)$ and $g(\eta)$ profiles decrease with an increase in α. Figure 4 to Figure 5 shows the effect of magnetic parameter M on the tangential velocity $f^{/}(\eta)$, transverse velocity $g(\eta)$ profiles, respectively. The velocity profile $f^{/}(\eta)$ decreases with an increase in the values of M, the same behavior has observed transverse velocity $g(\eta)$, As M increases, a drag force, called Lorentz force increases. Since this force opposes the flow of nanofluid, velocity in the flow direction decreases. Moreover, since an electrically conducting nanofluid with the strong magnetic field in the direction orthogonal to the

flow are considered, an increase in M increases the force in the z-direction which results in an diminishes in the transverse velocity profile g(η).

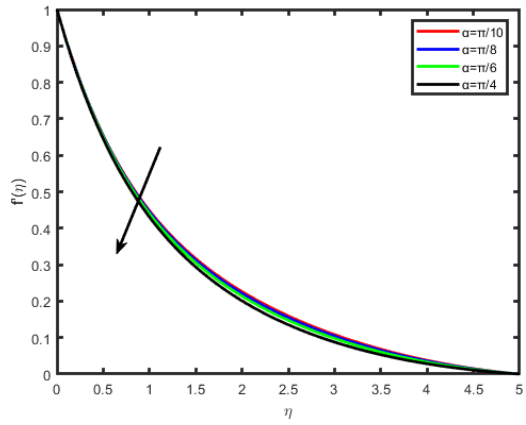

Fig. 2. Effect of α on f′(n)

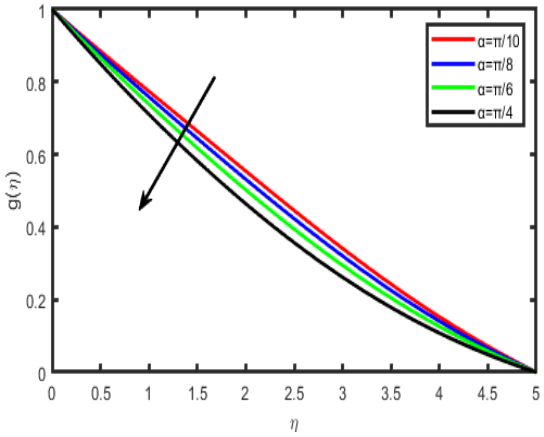

Fig. 3. Effect of α on g(n)

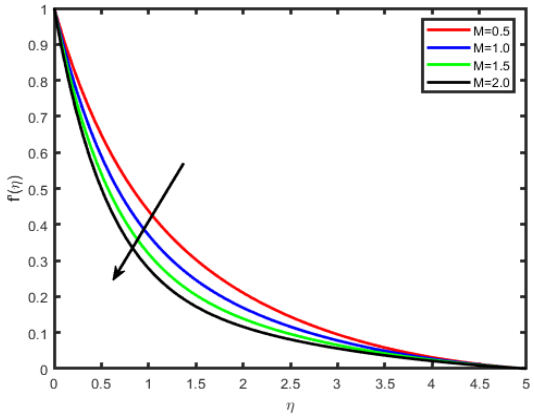

Fig. 4. Effect of M on f′(n)

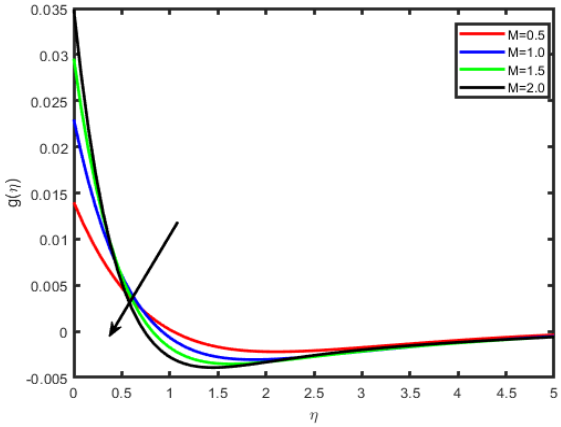

Fig. 5. Effect of M on g(n)

In Figure 6 to Figure 9 the effects of the thermal Grashof Grx and concentration Grashof Grc numbers on the tangential velocity $f'(\eta)$, and the transverse velocity g(η) respectively. As the Grashof number is a ratio of the buoyancy force to the viscous force and it appears due to the natural convection flow, so an increase in the tangential velocity as well as the lateral velocity of the fluid is observed when the thermal and the concentration Grashof numbers are increased as shown in Figure 6 to Figure 9. It happens because of the fact that higher the Grashof number implies higher the buoyancy force which means higher the movement of the flow.

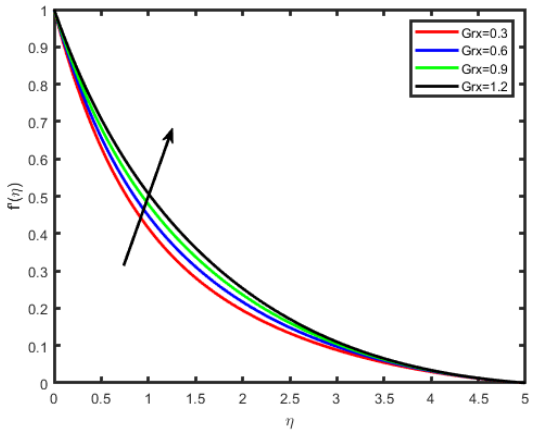

Fig. 6. Effect of Grx on f′(n)

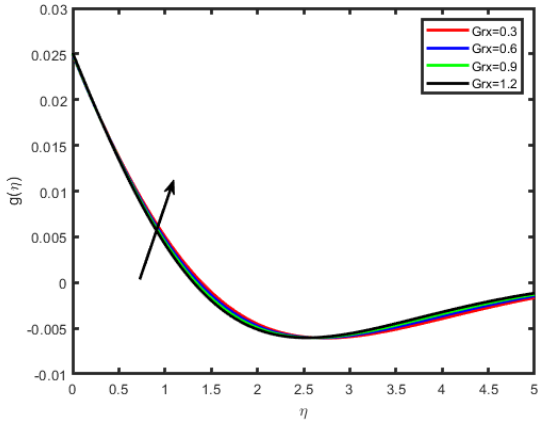

Fig. 7. Effect of Grx on g(n)

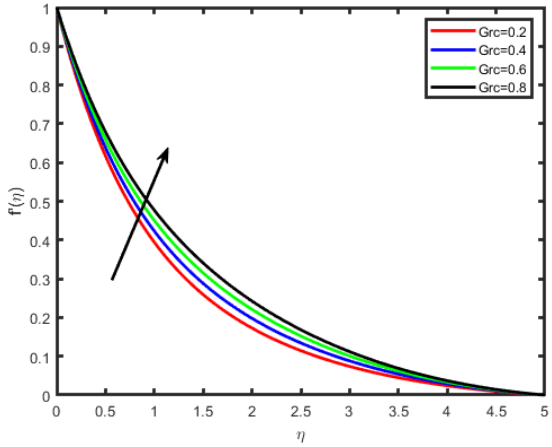

Fig. 8. Effect of Grc on f′(n)

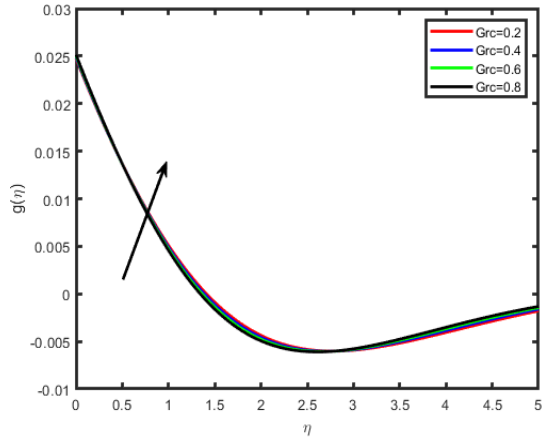

Fig. 9. Effect of Grc on g(n)

Figure 10 to Figure 13 illustrate the impacts of the Hall parameter m on tangential velocity $f^{i}(\eta)$, transverse velocity g(η), nanoparticle concentration ϕ(η) and temperature θ(η) profiles, respectively. It is observed that both the velocity f′(η) and g(η) profiles increase as m increases. But the temperature and concentration profiles decrease with an increase in m as shown in Figure 12 and Figure 13. This is because the enclosure of Hall parameter decreases the resistive force caused by the magnetic field due to its effect of reducing the effective conductivity. Hence, the velocity component increases as the Hall parameter increases.

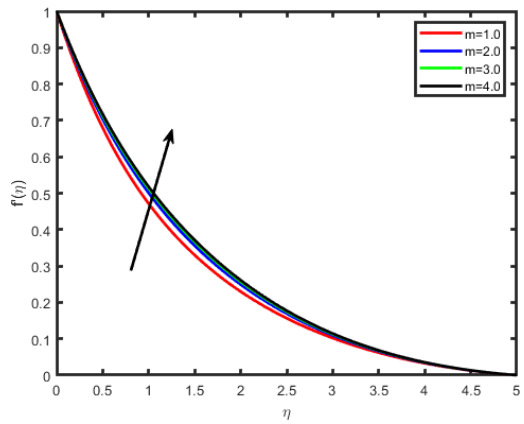

Fig. 10. Effect of m on f′(n)

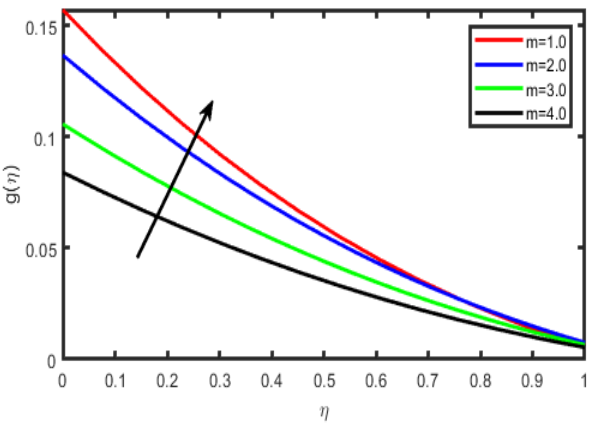

Fig. 11. Effect of m on g(n)

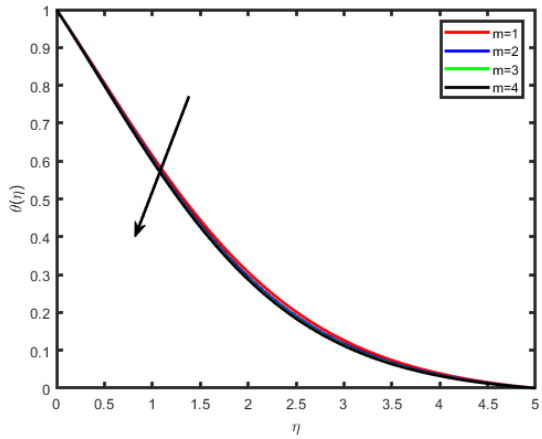

Fig. 12. Effect of m on θ(n)

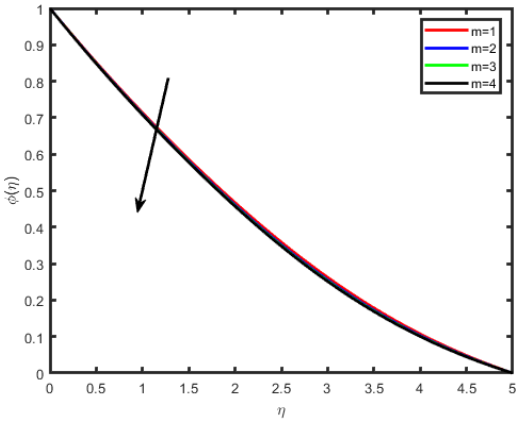

Fig. 13. Effect of m on φ(n)

Influence of Brownian motion parameter Nb on the temperature and concentration profiles is studied in Figure 14 and Figure 15. From these figures, we notice that an enhancement in the values of Nb gives rise to the temperature, while it causes a decrease in the nanoparticle concentration profile. Brownian motion is the random motion of nanoparticles suspended in the fluid, caused by the collision of nanoparticles with the fluid particles. An increment in the thermophoretic effect causes an increment in the Brownian motion effect which results in the rise of the temperature due to the increment in the kinetic energy. Figure 16 and Figure 17 illustrate the effect of thermophoresis parameter Nt on the temperature and the nanoparticles concentration profile. One can observe that temperature and concentration fields increase with an enhancement in Nt. Thermophoresis parameter plays an important role in the heat transfer flow. Thermophoresis force enhances when Nt is increased which tends to move the nanoparticles from the hot region to the cold and as a result the temperature and the boundary layer thickness increase.

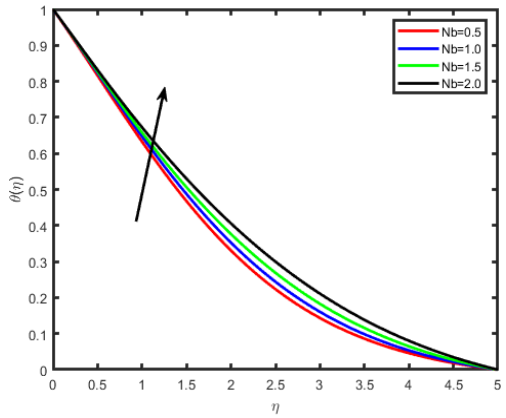

Fig. 14. Influence of Nb on θ(η)

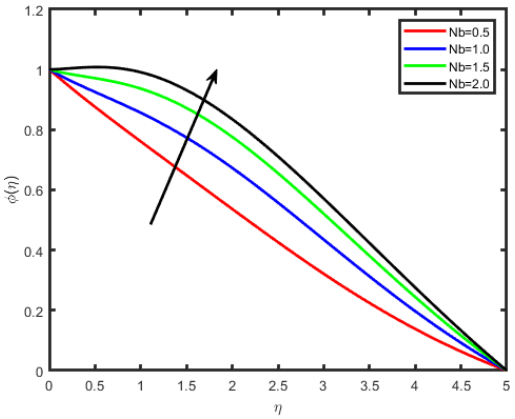

Fig. 15. Influence of Nb on ϕ(η)

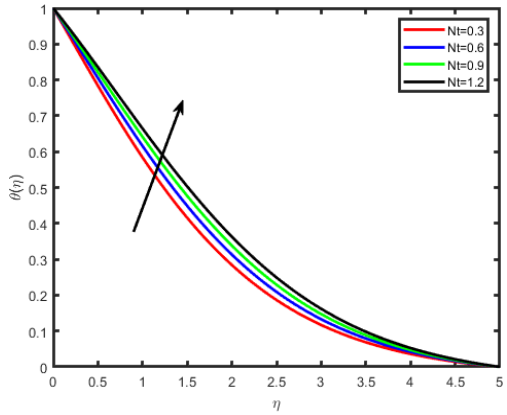

Fig. 16. Influence of Nt on θ(η)

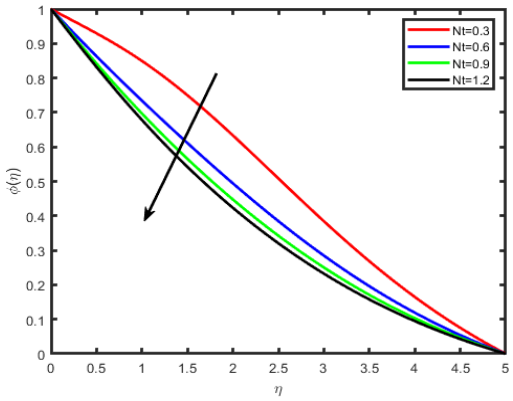

Fig. 17. Influence of Nt on ϕ(η)

Figure 18 depicts the effect of Dufour parameter on temperature profiles. As the Dufour parameter increases, the energy or temperature profiles increases. The Dufour number denotes the contribution of the concentration gradients to the thermal energy flux in the flow. It can be seen that an increase in the Dufour number causes a rise in temperature. The temperature curves for different values of thermal radiation parameter are depicted in Figure 19. From the graph, it is possible to observe that as the values of thermal radiation parameter upsurge, the temperature graph and the temperature boundary layer thickness are snowballing.

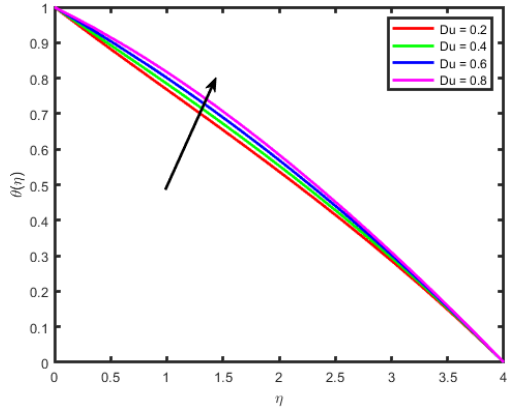

Fig. 18. Influence of Du on θ(η)

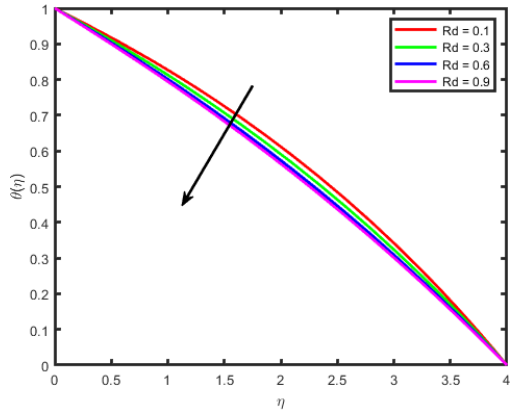

Fig. 19. Influence of Rd on θ(η)

Figure 20 envisage the activation energy (E) impact on concentration field. Graph elucidate that concentration profile increases for large value of E. The Arrhenius function deteriorations by snow balling the value of the activation energy, which outcomes in the promotion of the generative chemical reaction causing an improvement in the concentration field. Within the occurrence of low temperature and higher activation energy leads to a smaller reaction rate constant which slow down the chemical reaction. In this manner concentration profile boost up. Figure 21 show that when chemical reaction rate (σ) increases, concentration profile strongly reduces because of high chemical reaction rate which fallouts solute boundary layer becomes thicker. When σ increases steadily, the factor $(1+\Gamma\theta)\, e^{-E/(1+\Gamma\theta)}$ is enriches because of increase in values σ.

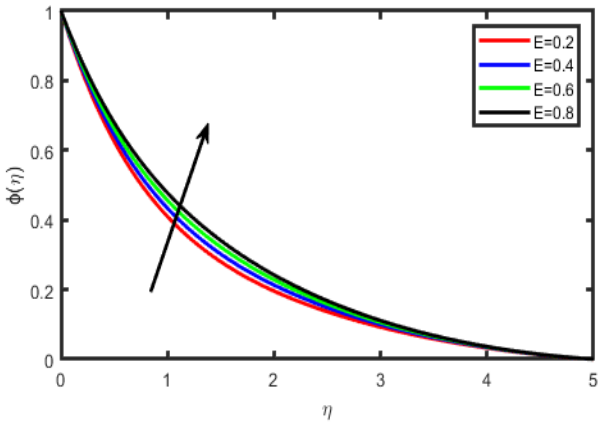

Fig. 20. Effect of (E) on Concentration φ(η)

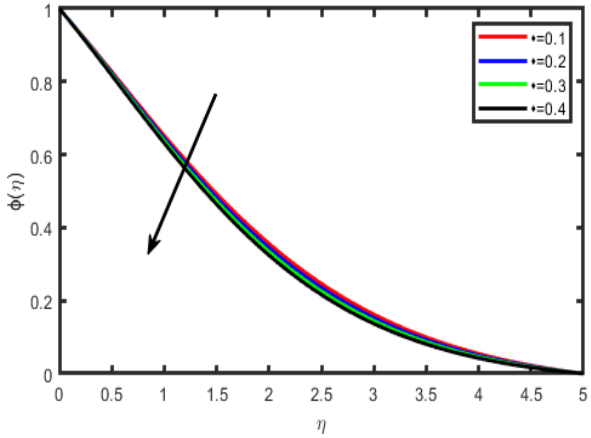

Fig. 21. Effect of (σ) on Concentration φ(η)

The impact of the various physical parameters on the local Sherwood number, skin friction coefficient and local Nusselt number, mathematical results are achieved for Nb= 0.3, α=π/3, Nt= 0.7, P r= 0.71, Le = 0.6, M= 0.5, m= 0.2, Grx = 0.5, Gr = 0.5, A*=0.01, B*= 0.01, and are enumerated as shown in Table 1. it is viewed that the skin-friction coefficient in x− direction decreases with an increase in the thermal Grashof number Grx, the mass Grashoff number Grc, Hall current parameter m, and Brownian motion parameter Nb, while it increases for the increasing value of magnetic parameter M and Prandtl number Pr, and thermophoresis parameter Nt. A completely opposite behavior is recorded for the coefficient of the skin-friction in the z-direction. Nusselt number increases when the Hall current parameter m, thermal Grashof number, the mass Grashoff number, and Prandtl number, increase whereas it is reduced by increasing the value of Magnetic field parameter M. Sherwood number has increasing behavior for thermal Grashof number Grx, Magnetic field parameter M, Brownian motion parameter Nb and thermophoresis parameter Nt, while it has decreasing behavior for Grashoff number Grc and Prandtl number.

Table 1

Numerical values of $\mathrm{Re}_x^{1/2} Cf_x$, $\mathrm{Re}_x^{1/2} Cf_z$, $\mathrm{Re}_x^{1/2} Nu_x$, $\mathrm{Re}_x^{1/2} Sh_x$

Grx	Grc	m	Nb	M	Pr	Nt	-2f''(0)	-2g'(0)	-θ'(0)	-ϕ'(0)
0.5							1.25478	0.85207	0.52125	0.90582
1.0							0.99784	0.91250	0.53273	0.9059
1.5							0.73549	0.95490	0.54596	1.09183
	0.3						0.98751	0.85167	0.50338	0.11084
	0.6						0.84756	0.98508	0.51293	0.11038
	0.9						0.71258	1.25267	0.57865	0.91095
		1					1.52142	0.85234	0.31435	0.81037
		2					1.02149	0.95408	0.29705	0.71945
		3					0.812575	0.99890	0.23127	0.91040
			0.2				0.95124	0.95209	0.84505	0.51095
			0.4				0.81523	0.96156	0.82157	0.61038
			0.6				0.71259	0.98542	0.80383	0.61845
				0.5			0.94524	1.02523	0.98706	0.71038
				1.0			1.24549	0.98503	0.91236	0.81037
				1.5			1.40350	0.85118	0.89505	0.904785
					0.68		0.97853	1.02103	0.12527	0.919037
					0.71		0.91203	0.98518	0.15753	0.991673
					0.76		0.84528	0.90393	0.19894	0.90274
						0.3	1.54529	0.98583	0.85438	0.52926
						0.6	1.12544	0.91269	0.81231	0.51835
						0.9	0.87521	0.89624	0.75234	0.67452

For the authentication of the numerical method used, the results were compared with the previously obtained results Ramudu *et al.,* [10] for various values of parameters and it indicates an excellent accord as shown in Table 2.

Table 2
Comparison of (f^{II} (0)) for various values of M when Nb= 0.3, Nt= 0.7, P r= 0.71, Le = 0.6, M= 0.5, Grx = 0.5, Grc= 0.5, A^*= B^*= 0.5, m= α= E=σ=0, Du=0

M	Ramudu *et al.,* [10]	Present values
0.5	-0.376895	-0.394674564
1.0	-0.5293058	-05973638934
1.5	-0.654598	-0659374748

7. Conclusion

The influence of the Activation Energy and Hall current on the heat and mass transfer of nanofluid flowing across a linearly stretched sheet is the topic that will be discussed in the present paper. The most significant accomplishments have been broken down into the following categories.

The temperature increases as the Brownian motion parameter (Nb) values increase, but the concentration profile of nanoparticles decreases. The temperature and concentration fields intensify with a rise in the Thermophoresis parameter (Nt). The impact of Diffusion thermo parameter (*Du)* on θ and φ are opposite. The concentration has increases with enhances of Activation energy (E) and the opposite behavior observed in the rate of chemical reaction. The temperature and concentration profiles tend to fall when the Prandtl number (Pr) is raised. The temperature increases by increasing Le while concentration decreases with an increase in the Lewis number. The velocity increases with enhance of hall parameter (m), whereas the reversal behavior has observed in the case of temperature and Concentration.

References

[1] Dullien, Francis A. L. *Porous media: fluid transport and pore structure*. Academic Press, 2012.
[2] Nield, Donald A., and Adrian Bejan. *Convection in porous media*. Springer, New York, 1999. https://doi.org/10.1007/978-1-4757-3033-3
[3] Noeld, D. A., and A. Beskok. *Micro Flows*. Springer, New York, 2002.
[4] Karniadakis, George Em, Ali Beskok, and Narayan Aluru. *Microflows and Nanoflows: Fundamentals and Simulation*. Vol. 29. Springer Science & Business Media, 2005.
[5] Forchheimer, P. H. "Wasserbewegung durch boden." *Zeitschrift des Vereines Deutscher Ingenieure* 45, no. 50 (1901): 1781-1788.
[6] Muskat, M. *The flow of homogeneous fluids through porous media*. McGraw-Hill, 1946.
[7] Kodi, Raghunath, Mohanaramana Ravuri, Nagesh Gulle, Charankumar Ganteda, Sami Ullah Khan, and M. Ijaz Khan. "Hall and ion slip radiative flow of chemically reactive second grade through porous saturated space via perturbation approach." *Waves in Random and Complex Media* (2022): 1-17. https://doi.org/10.1080/17455030.2022.2108555
[8] Raghunath, Kodi, G. Charankumar, and L. Giulio. "Effects of Soret, rotation, Hall, and ion slip on unsteady MHD flow of a Jeffrey fluid through a porous medium in the presence of heat absorption and chemical reaction." *Journal of Mechanical Engineering Research and Developments* 45, no. 3 (2022): 80-97.
[9] Raghunath, Kodi, and Ravuri Mohanaramana. "Hall, Soret, and rotational effects on unsteady MHD rotating flow of a second-grade fluid through a porous medium in the presence of chemical reaction and aligned magnetic field." *International Communications in Heat and Mass Transfer* 137 (2022): 106287. https://doi.org/10.1016/j.icheatmasstransfer.2022.106287
[10] Ramudu, Ankalagiri Chinna Venkata, Kempannagari Anantha Kumar, Vangala Sugunamma, and Naramgari Sandeep. "Heat and mass transfer in MHD Casson nanofluid flow past a stretching sheet with thermophoresis and Brownian motion." *Heat Transfer* 49, no. 8 (2020): 5020-5037. https://doi.org/10.1002/htj.21865

[11] Cheng, Ching-Yang. "Soret and Dufour effects on free convection heat and mass transfer from an arbitrarily inclined plate in a porous medium with constant wall temperature and concentration." *International Communications in Heat and Mass Transfer* 39, no. 1 (2012): 72-77. https://doi.org/10.1016/j.icheatmasstransfer.2011.09.003
[12] Hayat, Tasawar, Muhammad Ijaz Khan, Muhammad Waqas, and Ahmed Alsaedi. "Stagnation point flow of hyperbolic tangent fluid with Soret-Dufour effects." *Results in Physics* 7 (2017): 2711-2717. https://doi.org/10.1016/j.rinp.2017.07.014
[13] Postelnicu, Adrian. "Influence of a magnetic field on heat and mass transfer by natural convection from vertical surfaces in porous media considering Soret and Dufour effects." *International Journal of Heat and Mass Transfer* 47, no. 6-7 (2004): 1467-1472. https://doi.org/10.1016/j.ijheatmasstransfer.2003.09.017
[14] Kafoussias, N. G., and E. W. Williams. "Thermal-diffusion and diffusion-thermo effects on mixed free-forced convective and mass transfer boundary layer flow with temperature dependent viscosity." *International Journal of Engineering Science* 33, no. 9 (1995): 1369-1384. https://doi.org/10.1016/0020-7225(94)00132-4
[15] Alam, M. S., M. Ferdows, M. Ota, and M. A. Maleque. "Dufour and Soret effects on steady free convection and mass transfer flow past a semi-infinite vertical porous plate in a porous medium." *Applied Mechanics and Engineering* 11, no. 3 (2006): 535.
[16] Weaver, J. A., and R. Viskanta. "Natural convection due to horizontal temperature and concentration gradients-2. Species interdiffusion, Soret and Dufour effects." *International Journal of Heat and Mass Transfer* 34, no. 12 (1991): 3121-3133. https://doi.org/10.1016/0017-9310(91)90081-O
[17] Sheikholeslami, Mohsen, M. M. Rashidi, and D. D. Ganji. "Numerical investigation of magnetic nanofluid forced convective heat transfer in existence of variable magnetic field using two phase model." *Journal of Molecular Liquids* 212 (2015): 117-126. https://doi.org/10.1016/j.molliq.2015.07.077
[18] Abbasi, F. M., S. A. Shehzad, T. Hayat, A. Alsaedi, and Mustafa A. Obid. "Influence of heat and mass flux conditions in hydromagnetic flow of Jeffrey nanofluid." *AIP Advances* 5, no. 3 (2015): 037111. https://doi.org/10.1063/1.4914549
[19] Abel, M. Subhas, and Mahantesh M. Nandeppanavar. "Heat transfer in MHD viscoelastic boundary layer flow over a stretching sheet with non-uniform heat source/sink." *Communications in Nonlinear Science and Numerical Simulation* 14, no. 5 (2009): 2120-2131. https://doi.org/10.1016/j.cnsns.2008.06.004
[20] Sandeep, N., and C. Sulochana. "Dual solutions for unsteady mixed convection flow of MHD micropolar fluid over a stretching/shrinking sheet with non-uniform heat source/sink." *Engineering Science and Technology, an International Journal* 18, no. 4 (2015): 738-745. https://doi.org/10.1016/j.jestch.2015.05.006
[21] Sandeep, N. "Effect of aligned magnetic field on liquid thin film flow of magnetic-nanofluids embedded with graphene nanoparticles." *Advanced Powder Technology* 28, no. 3 (2017): 865-875. https://doi.org/10.1016/j.apt.2016.12.012
[22] Kumar, Anantha, V. Sugunamma, and N. Sandeep. "Numerical exploration of MHD radiative micropolar liquid flow driven by stretching sheet with primary slip: a comparative study." *Journal of Non-Equilibrium Thermodynamics* 44, no. 2 (2019): 101-122. https://doi.org/10.1515/jnet-2018-0069
[23] Ramadevi, B., V. Sugunamma, Anantha Kumar, and Ramana Reddy J. V. "MHD flow of Carreau fluid over a variable thickness melting surface subject to Cattaneo-Christov heat flux." *Multidiscipline Modeling in Materials and Structures* 15, no. 1 (2018): 2-25. https://doi.org/10.1108/MMMS-12-2017-0169
[24] Mahanthesh, B., B. J. Gireesha, and I. L. Animasaun. "Exploration of non-linear thermal radiation and suspended nanoparticles effects on mixed convection boundary layer flow of nanoliquids on a melting vertical surface." *Journal of Nanofluids* 7, no. 5 (2018): 833-843. https://doi.org/10.1166/jon.2018.1521
[25] Makinde, O. D., and I. L. Animasaun. "Thermophoresis and Brownian motion effects on MHD bioconvection of nanofluid with nonlinear thermal radiation and quartic chemical reaction past an upper horizontal surface of a paraboloid of revolution." *Journal of Molecular Liquids* 221 (2016): 733-743. https://doi.org/10.1016/j.molliq.2016.06.047
[26] Hinds, William C. *Aerosol technology: properties, behavior, and measurement of airborne particles*. John Wiley & Sons, 1982.
[27] Bakier, Yousof Ahmed, and Ahmed Mohamed Mansour. "Combined of magnetic field and thermophoresis particle deposition in free convection boundary layer from a vertical flat plate embedded in a porous medium." *Thermal Science* 11, no. 1 (2007): 65-74. https://doi.org/10.2298/TSCI0701065B
[28] Tsai, Chuen-Jinn, Jyh-Shyan Lin, Shankar G. Aggarwal, and Da-Ren Chen. "Thermophoretic deposition of particles in laminar and turbulent tube flows." *Aerosol Science and Technology* 38, no. 2 (2004): 131-139. https://doi.org/10.1080/02786820490251358
[29] Goldsmith, P., and F. G. May. "Diffusiophoresis and thermophoresis in water vapour systems." *Aerosol Science* (1966): 163-194.

[30] Goren, Simon L. "Thermophoresis of aerosol particles in the laminar boundary layer on a flat plate." *Journal of Colloid and Interface Science* 61, no. 1 (1977): 77-85. https://doi.org/10.1016/0021-9797(77)90416-7
[31] Sutton, George W., and Arthur Sherman. *Engineering magnetohydrodynamics*. McGraw-Hill, 1965.
[32] Abo-Eldahab, Emad M., and Mohamed A. El Aziz. "Hall and ion-slip effects on MHD free convective heat generating flow past a semi-infinite vertical flat plate." *Physica Scripta* 61, no. 3 (2000): 344. https://doi.org/10.1238/Physica.Regular.061a00344
[33] Buongiorno, Jacopo. "Convective transport in nanofluids." *ASME Journal of Heat and Mass Transfer* 128, no. 3 (2006): 240-250. https://doi.org/10.1115/1.2150834
[34] Chamkha, Ali J., and Abdul-Rahim A. Khaled. "Similarity solutions for hydromagnetic simultaneous heat and mass transfer by natural convection from an inclined plate with internal heat generation or absorption." *Heat and Mass Transfer* 37, no. 2-3 (2001): 117-123. https://doi.org/10.1007/s002310000131
[35] Abo-Eldahab, Emad M., and Mohamed A. El Aziz. "Blowing/suction effect on hydromagnetic heat transfer by mixed convection from an inclined continuously stretching surface with internal heat generation/absorption." *International Journal of Thermal Sciences* 43, no. 7 (2004): 709-719. https://doi.org/10.1016/j.ijthermalsci.2004.01.005